frontiers in Endocrinology

TYPE Original Research
PUBLISHED 23 March 2026
DOI 10.3389/fendo.2026.1764298

Check for updates

OPEN ACCESS

EDITED BY
Amjad Khan,
Chung-Ang University, Republic of Korea

REVIEWED BY
Stefano Stanca,
École des Hautes Études en Sciences Sociales, France
Sibah Hasan,
Neuro-Bio Ltd, United Kingdom

*CORRESPONDENCE
Dóra Zelena
zelena.dora@pte.hu

†These authors have contributed equally to this work

RECEIVED 09 December 2025
REVISED 24 February 2026
ACCEPTED 03 March 2026
PUBLISHED 23 March 2026

CITATION
Sólyomvári C, Makkai G, Capelo-Carrasco N, Strac DS, Zelena D and Farkas S (2026) Time-dependent histological characterization of amyloid-β induced cholinergic and glial alterations and their modulation by dehydroepiandrosterone sulfate (DHEAS).
Front. Endocrinol. 17:1764298.
doi: 10.3389/fendo.2026.1764298

COPYRIGHT
© 2026 Sólyomvári, Makkai, Capelo-Carrasco, Strac, Zelena and Farkas. This is an open-access article distributed under the terms of the Creative Commons Attribution License (CC BY). The use, distribution or reproduction in other forums is permitted, provided the original author(s) and the copyright owner(s) are credited and that the original publication in this journal is cited, in accordance with accepted academic practice. No use, distribution or reproduction is permitted which does not comply with these terms.

Time-dependent histological characterization of amyloid-β induced cholinergic and glial alterations and their modulation by dehydroepiandrosterone sulfate (DHEAS)

Csenge Sólyomvári[1,2], Géza Makkai[3], Nicolas Capelo-Carrasco[4,5,6], Dubravka Svob Strac[7], Dóra Zelena[1,2*†] and Szidónia Farkas[1,2†]

[1]Laboratory of Behavioral and Stress Studies, Institute of Physiology, University of Pécs, Pécs, Hungary, [2]Centre for Neuroscience, János Szentágothai Research Centre, University of Pécs, Pécs, Hungary, [3]Nano-Bio-Imaging Core Facility, University of Pécs, Pécs, Hungary, [4]Instituto de Biomedicina de Sevilla (IBiS), Hospital Universitario Virgen del Rocío/Centro Superior de Investigaciones Científicas (CSIC)/Universidad de Sevilla, Seville, Spain, [5]Centro de Investigación Biomédica en Red sobre Enfermedades Neurodegenerativas (CIBERNED), Madrid, Spain, [6]Department of Bioquímica y Biología Molecular, Facultad de Farmacia, Universidad de Sevilla, Seville, Spain, [7]Laboratory for Molecular Neuropsychiatry, Ruder Boskovic Institute, Division of Molecular Medicine, Zagreb, Croatia

Introduction: Alzheimer's disease (AD) is a multifactorial neurodegenerative disorder characterized by predominant - but not exclusive - pathological accumulation of amyloid-β (Aβ) in the brain. This process affects not only neurons (particularly cholinergic) but also glial cells, contributing to progressive neuronal loss and neuroinflammation. Dehydroepiandrosterone (DHEA) and dehydroepiandrosterone sulfate (DHEAS) are endogenous steroids that are hypothesized to exert neuroprotective and anti-inflammatory effects. This study aims to histologically characterize the *in vivo* temporal progression of Aβ-induced alterations in cholinergic neurons and glial morphology. Our secondary aim was to evaluate whether DHEAS protects cholinergic integrity and, if so, whether this effect is mediated through glial activation.

Methods: $A\beta_{1-42}$ was injected into the cholinergic nucleus basalis magnocellularis (NBM) region of C57BL6/J male mice and one hour later 10 mg/kg DHEAS or vehicle (0.9% saline) was applied intraperitoneally. After 3, 12 or 33 days, the mice were transcardially perfused and immunohistochemical staining was used to investigate cholinergic cell (ChAT) and fiber (AChE) loss, as well as microglia (IBA1) and astrocyte (GFAP) morphology.

Results: Our findings confirmed that Aβ peptide exerted neurotoxic effects on the cholinergic system and triggered time-dependent activation in both glia cell types. Microglial cells initiated their response by day 3, adopting an amoeboid morphology, whereas delayed astrocytic reactivity was observed between days 3 and 12, demonstrated by increased ramification. DHEAS treatment preserved cholinergic fiber density, without effecting the number of cell bodies and modulated the inflammatory responses of glia cells, by decreasing the area occupied and number of microglia in a time dependent manner.

Discussion: Aβ toxicity exerts time-dependent effects on both cholinergic neurons and glia cells, while DHEAS shows therapeutic promise, though its efficacy and exact mechanism require further investigation.

KEYWORDS

amyloid-β, astrocytes, cholinergic system, dehydroepiandrosterone sulfate (DHEAS), microglia, neuroinflammation, neurosteroids

1 Introduction

Alzheimer's Disease (AD) is the most common neurodegenerative disorder, with a complex etiology not yet fully understood. The deterioration of the cholinergic system, observed in AD, results in a significant decrease of acetylcholine (ACh). This neurotransmitter is essential for cognitive processes, such as learning and memory (1, 2). Evidence shows that the basal forebrain, especially the Meynert nucleus (in rodents the nucleus basalis magnocellularis complex, NBM) (2, 3), the brain's main source of acetylcholine, is significantly affected (4). A central event (alongside other contributing factors) that initiates the pathogenesis of AD might be the formation and accumulation of amyloid-beta (Aβ) oligomers. This plays a crucial role in driving cholinergic dysfunction and degeneration. In the human brain Aβ accumulates in multiple phases, with cholinergic basal forebrain neurons affected from phase 3. At this stage clinical cognitive decline typically emerges, underscoring the central role of plaques in the disease progression (5). Aging appears to exacerbate Aβ toxicity, with cholinergic neurons being especially vulnerable (6). Specifically, Aβ accumulation can decrease ACh synthesis and secretion (3, 7), as well as choline uptake (8). Moreover, acetylcholinesterase (AChE), the enzyme that rapidly breaks ACh at the axon terminals (2), can interact with Aβ peptides, promoting the formation of Aβ plaques and fostering neuronal death (9). The Aβ accumulation can also influence Ca^{2+} homeostasis, leading to further cell degeneration (10). These findings suggest that injection of Aβ into NBM, which leads to cholinergic cell death, can be used as a targeted model of AD-related neuronal toxicity (11).

Neuroinflammation, attributed to activated microglia and astrocytes, is considered as a driving force in the onset and progression of AD (12, 13). Glial cells respond to Aβ plaque formation by transitioning into reactive forms (14, 15). In the early stages of the disease, reactive glia plays a beneficial role in clearing Aβ. However, prolonged activation results in chronic inflammation, characterized by elevated levels of pro-inflammatory cytokines, such as tumor necrosis factor-α (TNFα), interleukins (IL-6, IL-1β) and nitric oxide (NO), with damaging effects on the nervous system (16). Microglia activation, driven by elevated levels of Aβ and reactive oxygen species (ROS), results in impaired Aβ phagocytosis (16). In parallel with this, reactive astrocytes undergo hypertrophy and overexpress markers such as glial fibrillary acidic protein (GFAP), nestin, and vimentin (16–19). In AD, astrocytes become more sensitive to Ca^{2+} signaling, reacting more rapidly and intensely and exhibiting increased ROS production. This reduces the levels of glutathione (GSH), one of the brain's most important antioxidants (20). Hence, mitigating inflammation could represent potential therapeutic approach to AD.

Dehydroepiandrosterone (DHEA) is an endogenous steroid that serves as a precursor for sex hormones testosterone and estrogen. It is primarily produced in adrenal glands and gonads (21, 22), but also synthesized in the central nervous system by neurons and glial cells (23, 24). DHEA is converted into its more stable, water-soluble, biologically active and major circulating form, dehydroepiandrosterone sulfate (DHEAS). Numerous studies have shown that both DHEA and DHEAS levels significantly decrease with age (25) and in AD (26–28). Our previous study showed that DHEAS mitigates Aβ-induced neurotoxicity by modulating mitochondrial function, apoptosis, and the PI3K/Akt–Bcl2 signaling pathway, and reduces Aβ plaque load in the motor cortex of 3xTg-AD mice (29). Due to its steroidal properties, it is hypothesized to exert neuroprotective and anti-inflammatory effects, which might be observed already after a single injection (24, 30, 31). Furthermore, DHEAS has been reported to modulate γ-Aminobutyric acid sub-type A receptors ($GABA_AR$) and N-methyl-D-aspartate (NMDA) receptor function (32, 33), influence neurotrophic factors such as brain-derived neurotrophic factor (BDNF) and nerve growth factor (NGF) (34), and exert antioxidant effects. Moreover, DHEA increased acetylcholine (ACh) release from hippocampal neurons (35), while evidence suggests that DHEAS, rather than DHEA, more effectively enhances central cholinergic function (36). Based on this premise, these compounds emerge as promising therapeutic candidates for neurodegenerative diseases; however; so far the supporting evidence is sparse and not conclusive, and the exact mechanisms of their actions are still not clear (24, 37).

Therefore, using unilateral $Aβ_{1–42}$ injection into the NBM as an animal model of AD, our aims were to (i) characterize $Aβ_{1-42}$-induced alterations in cholinergic neurons and glial cells and (ii) assess the modulatory effects of DHEAS. Although $Aβ_{1-42}$-induced neurotoxicity and inflammatory responses are well established, time-dependent alterations representing the progression of the processes are sparse, relying mostly on *in vitro* observations (38). In this study, animals were treated with water-soluble DHEAS one hour after the neurotoxic injection, and subsequent cellular and histological alterations were analyzed. Morphological examination was assessed 3, 12 and 33 days after the neurotoxic lesion, based on previous results from our laboratory demonstrating neuroprotective potential of estradiol in these timepoints (11).

2 Materials and methods

2.1 Animals

The study enrolled three-month-old male C57BL/6J mice, since a more prominent effect was expected in males due to the androgenic nature of DHEA and DHEAS (39). All animals were bred and housed at the University of Pécs, Medical School, Institute of Physiology. Mice were maintained under a 12 hours light/dark cycle (lights on at 10 a.m.) and provided food and water *ad libitum*. Mice (~25 g) were group-housed (5–6 per cage) in 325 × 170 × 140 mm cages. The temperature of the animal room was 22 ± 2 °C, and the relative humidity was 55 ± 10%. The number of animals was 6-8/group, in total 56. No mortality occurred during the study. All experiments were approved by the Workplace Animal Welfare Committee of the University of Pécs and the National Scientific Ethical Committee on Animal Experimentation of Hungary (BA02/2000-84/2022) and performed according to the European Community Council Directive recommendations for the care and use of laboratory animals (2010/63/EU). The authors complied with the ARRIVE guidelines.

2.2 Neurotoxic model, stereotaxic surgery

While Aβ injection into specific brain regions does not fully recapitulate all aspects of AD, compared to a genetic mouse line this neurotoxic model allows precise control over pathology and timing, allowing direct assessment of cholinergic and glial responses. In addition, the fact that NBM complex projects ipsilaterally to the somatosensory cortex (SSC) (40), enables comparison of the two hemispheres after unilateral $A\beta_{1-42}$ injection. This eliminates interindividual differences, and reduces the number of required animals. Whereas bilateral injection is necessary for behavioral assessment (e.g., memory-related and cognitive outcomes), in our histological analysis we used unilateral administration allowing the contralateral hemisphere to serve as an internal control. This neurotoxic model also addresses the limited NBM pathology observed in transgenic models, where amyloid deposition primarily occurs in cortical, hippocampal, and amygdala regions with minimal and late basal forebrain involvement (41–43), in contrast to humans, where the Meynert nucleus is severely affected (44).

$A\beta_{1-42}$ was dissolved in sterile TRIS (300 nM; #252859-500G, Merck-Sigma-Aldrich, Darmstadt, Germany, pH=7.14) and "aged" for 5 days at room temperature (RT), whereas 0.05 M sterile TRIS solution (pH=7.14) was used as a control. $A\beta_{1-42}$ or TRIS were unilaterally stereotaxically administered to the NBM in a volume of 5×0.2 µL along the DV coordinate, under a 100 mg/kg ketamine (#A31108, Calypsol 50 mg/mL, Gedeon Richter, Budapest, Hungary) and 10 mg/kg xylazine (#QN05CM92, Sedaxylan 20 mg/mL, Dechra, Northwich, UK) anesthesia (Figure 1B). Unilateral injection was performed because this study focused on

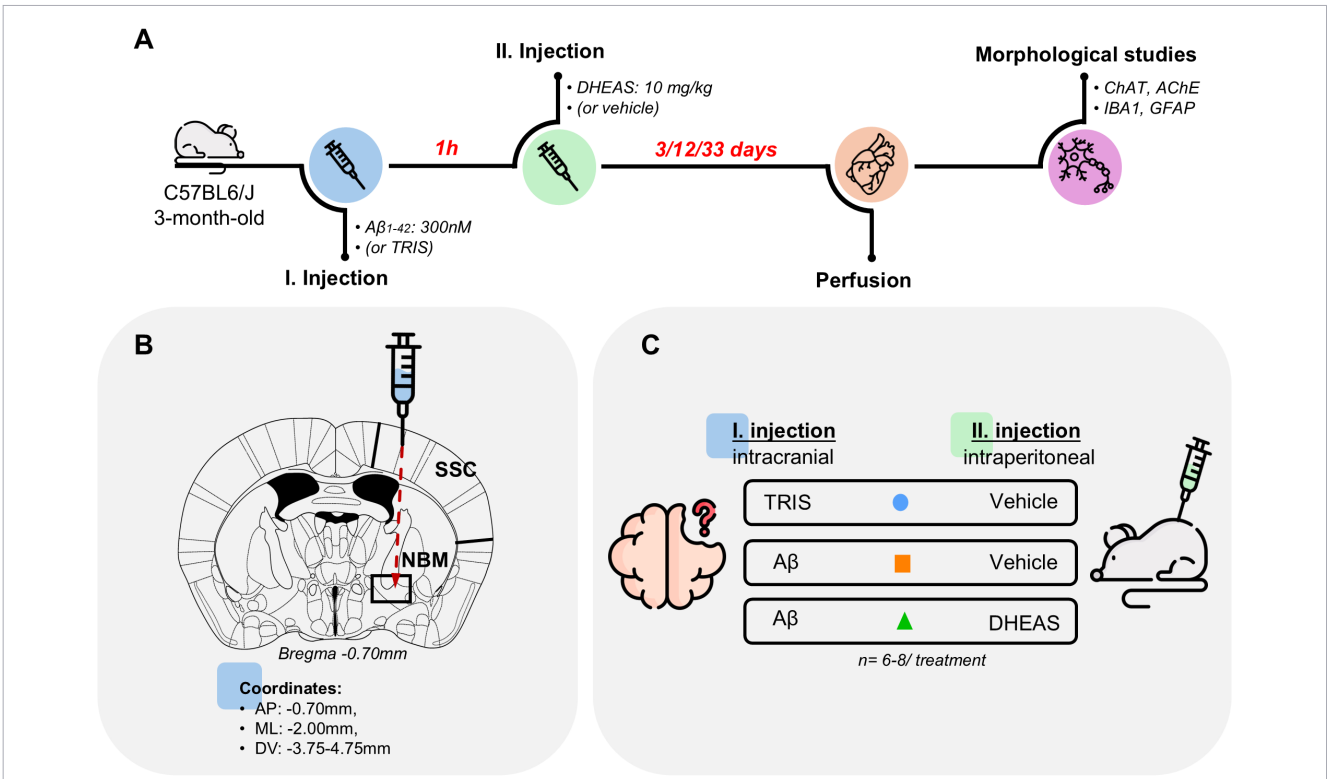


FIGURE 1
Experimental design. **(A)** The figure illustrates the chronological order of interventions, the time intervals between treatments **(red)** and the concentrations used. **(B)** Representative illustration of the stereotaxic surgery targeting the nucleus basalis magnocellularis (NBM), showing the stereotaxic coordinates and the projection area in the somatosensory cortex (SSC). **(C)** The various treatment groups. Other abbreviations: amyloid beta 1-42 ($A\beta_{1-42}$), tris(hydroxymethyl)aminomethane buffer (TRIS), dehydroepiandrosterone sulfate (DHEAS), choline acetyltransferase (ChAT), acetylcholinesterase (AChE), ionized calcium-binding adaptor molecule 1 (IBA1), glial fibrillary acidic protein (GFAP), number of animals (n). *Icons used in* Figure 1. Retrieved from https://www.flaticon.com/.

histological evaluation, with the contralateral hemisphere serving as a control. The stereotaxic coordinates from the bregma were: AP: -0.70 mm, ML: -2.00 mm, and DV: -3.75–4.75 mm (45). One hour after surgery, the animals received a single intraperitoneal (i.p.) injection of either vehicle (Veh, 10 mL/kg saline, 0.9% sodium chloride #07220-101-190, Molar Chemicals, Halásztelek, Hungary) or DHEAS (10 mg/kg; #SLBF3469V, Merck-Sigma-Aldrich, USA), (Figures 1A, C). Following three different time points (3, 12, 33 days after DHEAS treatment), the animals were anesthetized with an i.p. injection of a ketamine-xylazine cocktail (see above), and transcardially perfused with 15 mL of 0.9% sodium chloride solution, followed by 30 mL of 4% paraformaldehyde (PFA; #28794.295, VWR, Radnor, PA, USA), (Figure 1A). Brains were dissected and postfixed in 4% PFA for 3 hours and then dehydrated with 30% sucrose solution (#S9378-1KG, Merck-Sigma–Aldrich, Darmstadt, Germany) overnight. Coronal, 30 μm brain slices were made by a freezing microtome (SM2010 R, Leica, Chicago, IL, USA). The injection site was evaluated in all analyzed mice. Stereotaxic injections were performed using a fine glass capillary, which did not lead to visible, macroscopic changes, only to a small, cortical lesions (representative images are shown in Supplementary Figure 1).

2.3 Morphological staining

2.3.1 Choline acetyltransferase

Brain slices were selected from the coordinates: bregma -0.50 mm to -0.80 mm (45). Samples were washed with 0.05M TRIS for 3x10 minutes after each step. Endogenous peroxidase was blocked by a 3% peroxide solution (H_2O_2, #H1009-100mL, Merck-Sigma-Aldrich, Darmstadt, Germany) for 15 minutes. A background blocking mixture (containing 0.2% Triton X-100, #20540, Renal Labor, Budapest, Hungary; 10% horse serum (HS), #H1270-100ML and 0.05M TRIS) was then applied to the samples for 2 hours. After blocking, slices were incubated for 72 hours with the primary antibody ChAT (Goat, 1:1,000; #AB144P, Millipore, Burlington, MA, USA; 0.02% TX; 5% HS in TRIS). Next, brain slices were incubated with a biotinylated secondary antibody (biotinylated anti-goat 1:200, #705-065-147, Jackson ImmunoResearch, Cambridge, UK, 0.02% TX; 5% HS in TRIS) at RT for 2 hours. An avidin–biotin kit (VECTASTAIN Elite ABC-Peroxidase Kits, PK-6100, Vector Laboratories, Newark, PA, USA) diluted in 0.02% TX; 5% HS and 0.05M TRIS was applied for 2 hours, RT. The visualization was performed by Ni-DAB (3,3'-diaminobenzidine tetrahydrochloride hydrate, #D5637-1G; nickel (II) sulfate hexahydrate, #227676-500G; D-(+)-Glucose, #G8270-1KG and ammonium chloride, #213330-500G, Merck-Sigma–Aldrich, Darmstadt, Germany) and glucose oxidase (#G7141-10KU, Merck-Sigma–Aldrich, Darmstadt, Germany). Imaging was performed using a Nikon Eclipse E1 R (Nikon, Tokyo, Japan) microscope at 4x magnification.

2.3.2 Acetylcholinesterase histochemistry

To label the cholinergic fibers in the SSC an AChE histochemistry was performed (Figure 1B) (11). Slices were selected from the coordinates: bregma +0.10 mm to −0.70 mm (45). The first step of the staining process was a 5x1 minute sodium acetate (0.1M, pH 6; #S2889-250G, Merck-Sigma–Aldrich, Darmstadt, Germany) wash. Brain slices were then incubated 2x45 minutes in a mixture of sodium acetate buffer containing: acetylthiocholine iodide (0.05%; #A5751-1G, Merck-Sigma–Aldrich, Darmstadt, Germany), sodium citrate (0.1M; #S1804-500G, Merck-Sigma–Aldrich, Darmstadt, Germany), copper sulfate (0.03M; #209198-100G, Merck-Sigma–Aldrich, Darmstadt, Germany), and potassium ferricyanide (5mM; #244023-500G, Merck-Sigma–Aldrich, Darmstadt, Germany). The incubation was followed by a 5×1 minute sodium acetate wash. After that an ammonium sulfide (1%; #S7482142 737, Molar chemicals, Halásztelek, Hungary in sodium acetate) and then a silver nitrate mixture (1%; #S8157-10G, Merck-Sigma–Aldrich, Darmstadt, Germany, in sodium nitrate 0.1 M; #S8170-250G, Merck-Sigma–Aldrich, Darmstadt, Germany) was added. Next, the samples were washed for 5×1 minutes in sodium nitrate, followed by addition of sodium acetate. Imaging was performed using a Nikon Eclipse E1 R (Nikon, Tokyo, Japan) microscope at 10× magnification.

2.3.3 Fluorescent immunohistochemistry (IBA1, GFAP)

For the examination of microglia and astrocyte morphology, the injection site was selected between bregma -0.50 mm and -0.80 mm. We analyzed the NBM and the puncture channel separately, since the latter received no or very little amount of $A\beta_{1-42}$ but showed signs of mechanical tissue damage. During the staining, the samples were washed with 0.05M TRIS for 3x10 minutes after each step. Prior incubation of samples with primary antibodies (Ionized calcium-binding adaptor molecule 1 (IBA1), rabbit, 1:1000, #019-19741, FujiFilm Wako; GFAP: 1:1000 chicken, #NBP1-05198, Novus Biologicals), background blocking was performed (same as for ChAT staining). After 72 hour incubation with the primary antibodies, Alexa Fluor conjugated secondary antibodies (Alexa Fluor (A) A674, anti-rabbit, 1:2000, #711-605-152, Jackson ImmunoResearch; A488, anti-chicken, 1:2000, #5414658300, Eugene. OR, USA) were used. Slices were incubated with secondary antibodies for 2 h at RT. Cell nuclei were stained with Hoechst 33342 trihydrochloride trihydrate (#H3570, Invitrogen, Waltham, MA, USA). After coverslipping with ProLong Gold Antifade mounting medium (#P36934, Invitrogen, Waltham, MA, USA), imaging was performed using a Nikon Eclipse Ti2-E microscope with a Nikon C2 confocal detector (Nikon, Tokyo, Japan).

2.4 Image analysis

Images were analyzed using ImageJ (FIJI; National Institutes of Health, USA; version 1.54f) or CellProfiler (version 4.2.8; https://cellprofiler.org) software. All experimenters were blinded to the treatment groups.

To assess the cholinergic system, $ChAT^+$ cells were counted manually on both the lesioned and non-lesioned brain hemispheres, whereas for $AChE^+$ fibers the integrated optical density (IOD) was

quantified between layers IV and V of the SSC, as previously described (46).

For glial reactivity, the area occupied by glial cells was measured in ImageJ. Images were acquired under identical fixed settings, regardless of animal or condition. Brightness was adjusted using the "Window/Level" function, followed by conversion to 8-bit format and color inversion. After thresholding, a binary mask was created, and the "Analyze Particles" function was applied to quantify the total area occupied by the signal of interest.

For detailed morphological analysis, CellProfiler software was used. $GFAP^+$ and $IBA1^+$ signals were first detected and co-localized with DAPI to confirm that the analyzed objects represented cells. A minimum overlapping threshold of 10% was applied during co-localization analysis to define positive cells, ensuring that only objects with sufficient spatial overlap between immunofluorescent markers and DAPI-stained nuclei were included in subsequent analyses. Filtered objects were skeletonized, and the following parameters were extracted:

Cell count = the total number of segmented cells identified by co-localization with DAPI.

Perimeter = the total length of the cell boundary (in pixels).

Number of branches = the number of distinct cellular processes extending from the cell body.

Number of endpoints = the number of terminal ends of cellular processes.

Due to the unilateral injection, we compared the lesioned side with the intact brain hemisphere. We calculated a ratio for all parameters except for astrocyte morphology.

$$Ratio = lesion\ \ side / intact\ \ side$$

Since reactivity on the contralateral side was low or showed no GFAP reactivity at all, normalizing to the mean of the control group would affect the time-dependent analysis, therefore for astrocyte morphology we used the raw data from the injected hemisphere.

2.5 Statistical analysis

Statistical analysis was performed using GraphPad Prism version 8.0.1 (GraphPad software, Inc., San Diego, CA, USA). Sample size (n=6–8 per group) was determined based on power analysis. Power analysis was performed using G*Power 3.1 for a two-way ANOVA with treatment and time as factors. Assuming α=0.05, power=0.8, 2 levels of treatment, 3 time points, and a medium effect size (f=0.50), the minimum required sample size was estimated at n=6 per group per time point. To account for potential variability, we used n=6–8 animals per group. Outliers were identified using Dixon's Q test, and only statistically significant ones were excluded. Normality was assessed using the Shapiro–Wilk and Kolmogorov–Smirnov tests. Two-way ANOVA test (with factors treatment and time) was applied for group comparisons, and Tukey HSD test was used for *post-hoc* analysis. Pearson's correlation was calculated between cell loss and glia markers. Data is presented as mean ± SEM. A significant difference was accepted at $p<0.05$.

3 Results

3.1 Morphological assessment of the cholinergic system

To examine the cholinergic cell bodies, $ChAT^+$ cells were counted in the NBM (Figure 2A). The results demonstrated significant difference between groups (treatment: $F_{(2,45)}=3.729$, $p=0.0317$); but no significant time effect ($F_{(2,45)}=2.094$, $p=0.1351$) or interaction ($F_{(4,45)}=1.037$, $p=0.3988$), (Figures 2B, D). The significant $A\beta_{1\text{-}42}$-induced cell loss was detectable only at 12 days (TRIS+Veh. vs Aβ+Veh: $p=0.0398$; TRIS+Veh. vs Aβ+DHEAS: $p=0.0416$) and cholinergic cell number remained low 33 days post-injury. However, DHEAS treatment did not exert a protective effect against cholinergic cell death at any of the examined time points.

We further investigated the density of $AChE^+$ fibers in the SSC, the projection area of NBM neurons. We observed significant time ($F_{(2,49)}=3.748$, $p=0.0306$) and treatment ($F_{(2,49)}=3.187$, $p=0.0500$) effects, as well as their significant interaction ($F_{(4,49)}=2.774$, $p=0.0372$), (Figures 2C, E). Specifically, although three days after the $A\beta_{1\text{-}42}$-lesion no changes in fiber density were detected, after 12 days the $A\beta_{1\text{–}42}$ injection significantly reduced the relative fiber density compared to control group ($p=0.0034$). By day 33, the $A\beta_{1\text{-}42}$ -induced fiber density decrease showed signs of spontaneous improvement. DHEAS treatment significantly reduced the extent of AChE fiber degeneration 12 days following $A\beta_{1\text{-}42}$-lesion ($p=0.0024$).

3.2 Glial coverage in the cortex

During morphological investigation of glia cells, we first examined the injection-induced mechanical injury in the cortex. Our analysis revealed significant differences across time in both glial cell types: microglia and astrocytes (IBA1: $F_{(2,50)}=15.95$, $p<0.0001$; GFAP: $F_{(2,49)}=7.907$, $p=0.0011$, respectively), (Figures 3B, C; Supplementary Figure 2. for representative images). The $IBA1^+$ cells demonstrated a higher area occupancy on day 3 (3 days vs. 12 days: $p<0.0001$; 3 days vs. 33 days: $p=0.0002$), which has been reduced to day 12, remaining low also on day 33. In contrast, $GFAP^+$ cells showed the highest area coverage on day 12 (3 days vs. 12 days, $p=0.4007$), which decreased in day 33 (12 days vs. 33days, $p=0.0007$), (Figure 3C). There were no significant effects of treatment or significant interaction between treatment and time at any time point, which is in accordance with the fact that the $A\beta_{1\text{-}42}$-lesion was not induced in the cortex (Figures 3B, C). Furthermore, the DHEAS treatment had no effect on mechanical injury-induced glial reactivity in the cortex.

3.3 Glial coverage in the NBM

In the NBM both glial cell types, microglia and astrocytes, showed significant time-related differences (IBA1: $F_{(2,51)}=16.87$, $p<0.0001$; GFAP: $F_{(2,51)}=33.34$, $p<0.0001$), (Figures 3A, D, E),

10.3389/fendo.2026.1764298

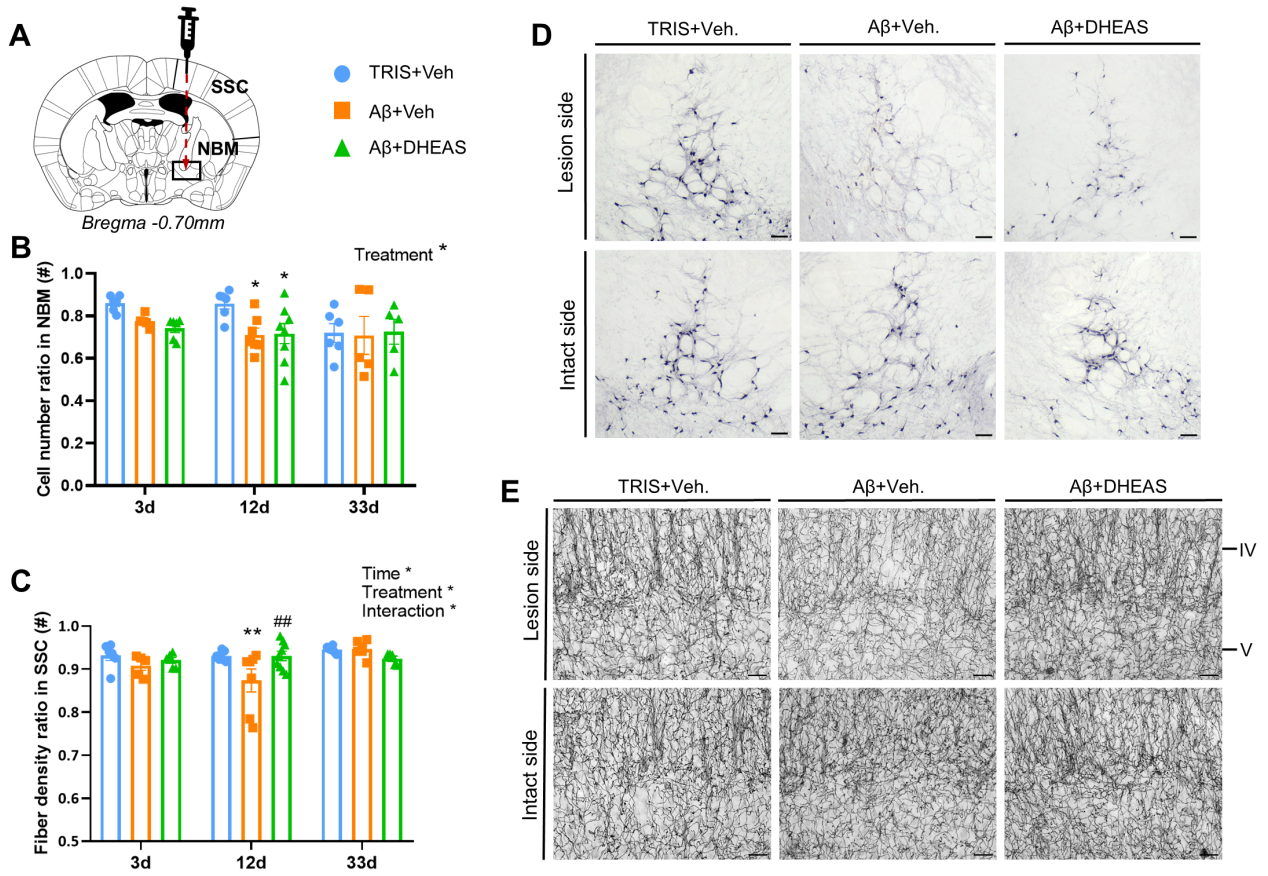


FIGURE 2
Immunohistochemical analysis of cholinergic cells and fibers. **(A)** Representative figure of the anatomical regions investigated. **(B)** Cell number changes across groups in the nucleus basalis magnocellularis (NBM). Slight decrease at 3 days post-Aβ, with significant loss by day 12 in both Aβ groups, persisting at day 33. **(C)** Changes in acetylcholinesterase (AChE) fiber density in somatosensory cortex (SSC). No change on day 3; reduced at day 12. Dehydroepiandrosterone sulfate (DHEAS) was effective and increased fiber density on day 12. On day 33, fiber degeneration showed an improving tendency, without any effect of the treatment. **(D)** Representative images of the immunohistochemical staining of choline-acetyltransferase (ChAT) positive cells on the lesioned and intact sides in the 12 days group. **(E)** Representative images of histochemical staining of AChE fibers on the lesioned and intact sides in the 12 days group. Cortical layers IV and V are visualized. Data are expressed as mean ± SEM. Differences compared to the TRIS+Veh. group are marked with asterics (*) *p<0.05, **p<0.01; while comparison to Aβ+Veh is marked with the number sign (#), ##p<0.01. Sample size is 6–8 animal/group. Scale bar: 20μm in D and 50μm in E.

mirroring the cortical pattern (Supplementary Figure 2. For representative images). Area covered by microglia cells demonstrated a general decline over time, being the highest on day 3 (3 days vs. 12 days, p<0.0001; 3 days vs 33 days, p<0.0001), whereas astrocyte coverage peaked on day 12 (3 days vs. 12 days, p<0.0001; 12 days vs 33 days, p<0.0001). The findings showed that in the NBM, $A\beta_{1-42}$ treatment resulted in a time-dependent glia reactivity (IBA1: $F_{(2,51)}$=13.84, p<0.0001; GFAP: $F_{(2,51)}$=4.829, p=0.0120; interaction: IBA1: $F_{(4,51)}$=3.751, p=0.0095; GFAP: $F_{(4,51)}$=2.971, p=0.0279) (Figures 3D, E). Specifically, the $A\beta_{1-42}$ injection significantly increased the area covered by $IBA1^+$ cells (microglia) on days 3 (TRIS+Veh. vs Aβ+Veh: p=0.0007), with a smaller increase on day 12 (TRIS+Veh. vs Aβ+Veh: p=0.0019) and no significant effect at day 33 (Figure 3D). On the other hand, DHEAS treatment significantly reduced the area covered by $IBA1^+$ cells on day 12 (Aβ+Veh vs. Aβ+DHEAS: p=0.0272). In the case of astrocytes, no significant difference was observed in the covered area 3 days after $A\beta_{1-42}$ or following DHEAS administration (Figure 3E). However, after 12 days, $A\beta_{1-42}$ injection increased the area occupied by $GFAP^+$ cells (TRIS+Veh. vs Aβ+Veh: p=0.0001) without significant effect of DHEAS treatment (TRIS +Veh vs. Aβ+DHEAS: p=0.0007, Aβ+Veh vs. Aβ+DHEAS: p=0.7797). By day 33 we observed a general decrease in the coverage of $GFAP^+$ astrocytes in the NBM.

3.3.1 Detailed morphology of the $IBA1^+$ microglia

At the site of injection (i.e., in the NBM) $A\beta_{1-42}$ administration increased the relative $IBA1^+$ cell number at 12 days (TRIS+Veh. vs Aβ+Veh: p=0.0254), (Figure 4C), which was not detected in any other group (i.e., 3 or 33 days and at 12 days: TRIS+Veh. vs Aβ+DHEAS treated: p=0.6949). All other investigated morphological parameters of the $IBA1^+$ microglia showed time-dependent changes (relative perimeter: $F_{(2,51)}$=9.035, p=0.0004; interaction: $F_{(4,51)}$=3.594, p=0.0117; relative number of branches: $F_{(4,51)}$=9.403, p=0.0003; relative number of branch endpoints: $F_{(2,50)}$=6.392, p=0.0034; Supplementary Figure 2. for representative images), with no differences observed on day 33 after $A\beta_{1-42}$ injection. On day 3, treatment, more specifically the $A\beta_{1-42}$ injection reduced the perimeter of the microglia cells ($F_{(2,51)}$=3.758, p=0.0300; TRIS+Veh.

10.3389/fendo.2026.1764298

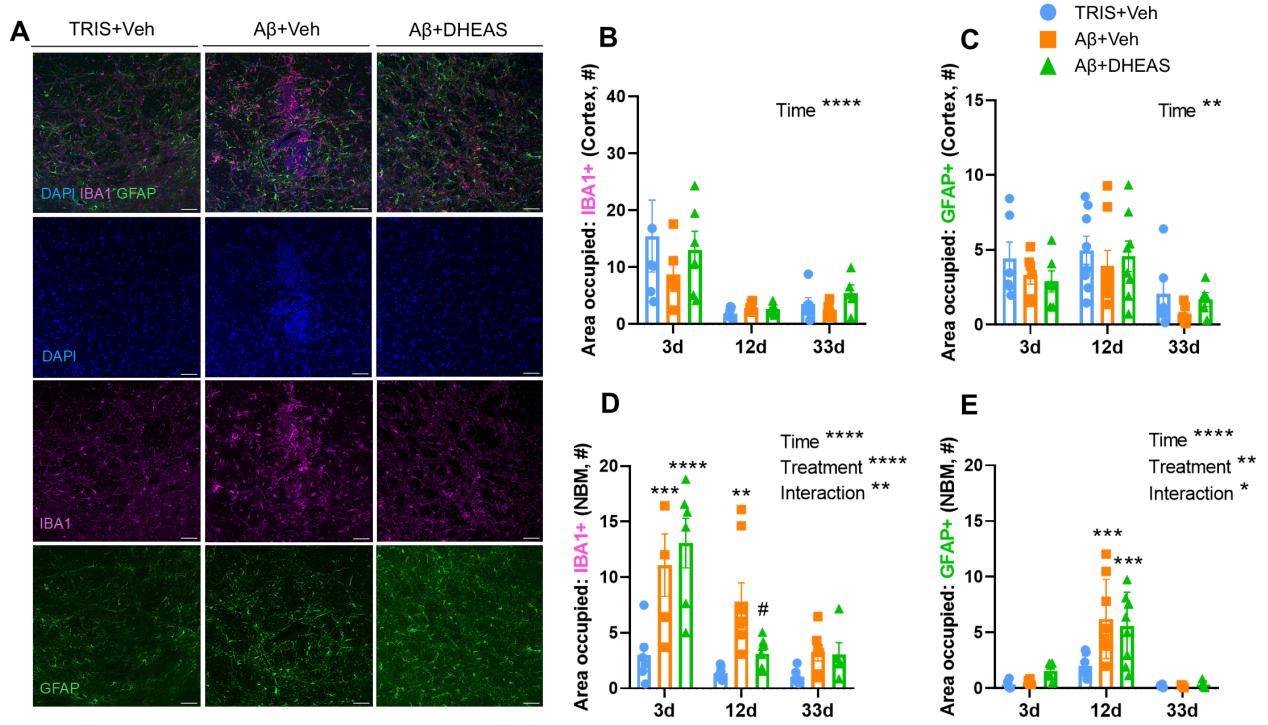


FIGURE 3
The effects of stereotaxic surgery on glia cell coverage, in the cortex and nucleus basalis magnocellularis (NBM). **(A)** Representative confocal images of the Aβ microinjection in the NBM on day 12 (labels: glial fibrillary acidic protein (GFAP), Ionized calcium-binding adaptor molecule 1 (IBA1). **(B)** Area occupied by microglia cells (IBA1) at different times after the mechanical injury in the cortex. Differences were only seen over time, with no significant variation between treatment groups. The area covered peaked on day 3 and steadily decreased to day 12 and 33. **(C)** Area occupied by astrocyte cells (GFAP) at different times. The coverage peaked on day 12 post-injection and decreased entirely by day 33. No effect of dehydroepiandrosterone sulfate (DHEAS) was detected in the cortical region. **(D)** Area occupied by microglia cells (IBA1) in the NBM. A significant increase in area coverage was observed after Aβ injection in both the 3 day and 12 days groups. However, dehydroepiandrosterone sulfate (DHEAS) reduced inflammation only at 12 days post-treatment. By day 33, we found no significant differences between the groups. **(E)** Area occupied by astrocyte cells (GFAP) in the NBM. A significant increase in astrocytic coverage was seen only 12 days post Aβ injection. By day 33, the area occupied by astrocytes decreased. No DHEAS effects were detected. Data are expressed as mean ± SEM. Differences compared to the TRIS+Veh. group are marked with asterics (*), *p<0.05; **p<0.01; ***p<0.001; ****p<0,0001. while comparison to Aβ-Veh is marked with the number sign (#) #p<0.05. Sample size is 6–8 animal/group. Scale bar: 200μm.

vs Aβ+Veh: p=0.0044), the number of branches ($F_{(2,51)}$=18.47, p<0.0001; TRIS+Veh. vs Aβ+Veh: p<0.0001), or the number of branch endpoints ($F_{(2,50)}$=6.794, p=0.0025; TRIS+Veh. vs Aβ+Veh: p=0.0131). However, DHEAS did not exert any significant effects on microglia perimeter (TRIS+Veh vs. Aβ+DHEAS: p=0.0014), (Figure 4D), the number of branches (TRIS+Veh vs. Aβ+DHEAS: p=0.0001), (Figure 4E), or the number of branch endpoints (TRIS +Veh vs. Aβ+DHEAS: p= 0.8329), (Figure 4F) on day 3. Similar alteration, albeit with a lower magnitude, was detected on day 12 (TRIS+Veh. vs Aβ+Veh: p=0.0126; TRIS+Veh vs. Aβ+DHEAS: p= 0.0324).

3.3.2 Detailed morphology of the GFAP+ astrocytes

In case of the astrocytes, all examined morphological parameters in the NBM showed time-dependent changes (cell number: $F_{(2,48)}$ =5.867, p=0.0053; perimeter: $F_{(2,39)}$=8.001, p=0.0012; relative number of branches: $F_{(2,49)}$=6.043, p=0.0045; relative number of branch endpoints: $F_{(2,48)}$=5.935, p=0.0050), (Figures 5B–E; Supplementary Figure 2. for representative images), with the highest values on day 12 post-injection. Treatment, more specifically $A\beta_{1-42}$ injection significantly increased the number of cells ($F_{(2,48)}$=3.484, p=0.0387; TRIS+Veh. vs Aβ+Veh: p=0.0037), (Figure 5B), the number of branches (TRIS+Veh. vs Aβ+Veh: p=0.0141), (Figure 5D) and the number of branch endpoints (TRIS+Veh. vs Aβ+Veh: p=0.0090), (Figure 5E) on day 12, without significant effects of DHEAS on the number of cells (TRIS+Veh vs. Aβ+DHEAS: p=0.0069), (Figure 5B), the number of branches (TRIS+Veh vs. Aβ+DHEAS: p=0.0175), (Figure 5D), or the number of branch endpoints (TRIS+Veh vs. Aβ+DHEAS: p=0.0128), (Figure 5E). On the other hand, analysis of the relative perimeter revealed no significant differences between the groups.

3.4 Correlation between cholinergic cell loss and glia markers

At day 3, the correlations between cholinergic cell loss in the NBM and certain microglial parameters (specifically the number of branches and endpoints, both p<0.01) were positive, whereas the correlations with astroglial parameters (all studied, p ≤ 0.01) were negative (Supplementary Table 1). At day 12, no significant correlation was found between cholinergic cell loss in the NBM and any of the glial parameters examined. By day 33, the GFAP-based parameters were positively correlated with cell loss (all parameters, at least p<0.05; Supplementary Table 1).

10.3389/fendo.2026.1764298

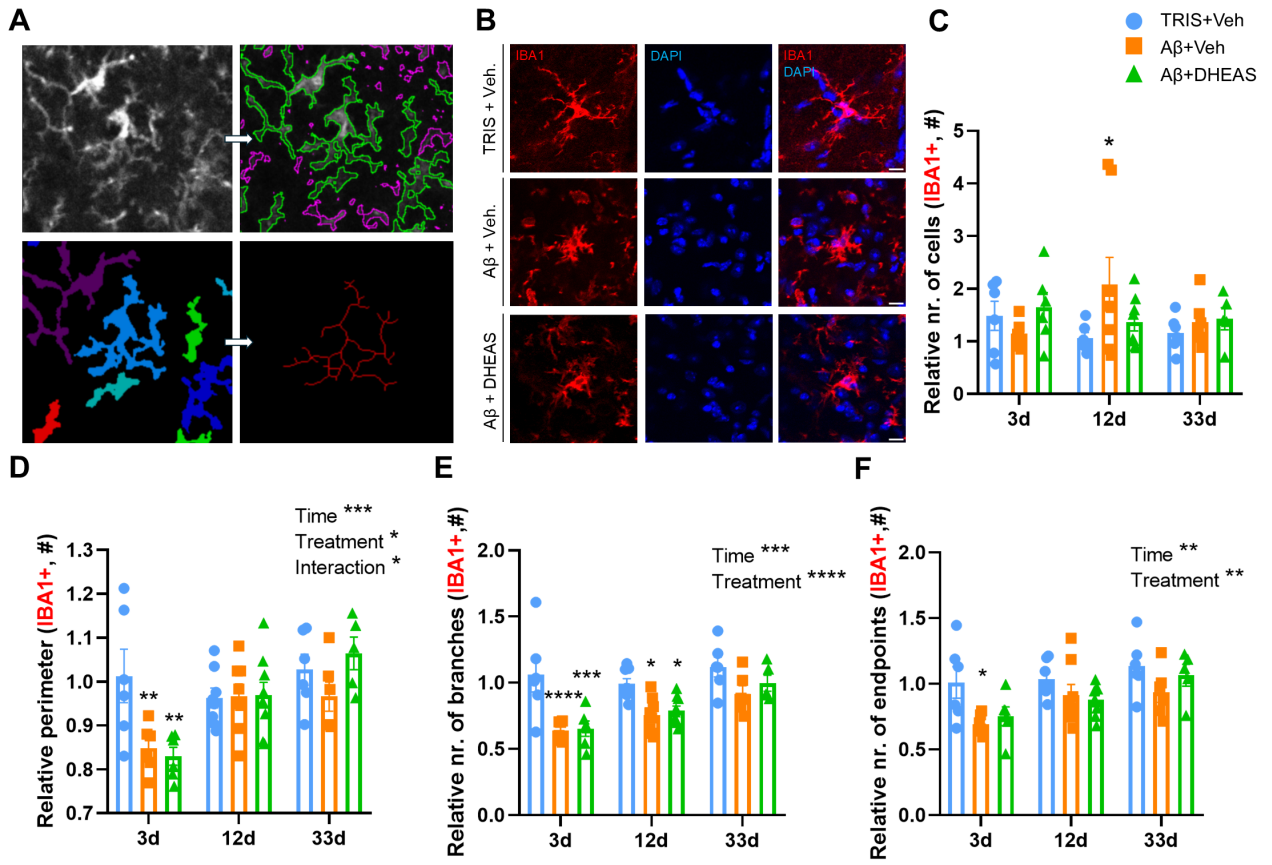


FIGURE 4
Microglia (IBA1) cell morphology in the nucleus basalis magnocellularis (NBM): **(A)** Representative figure showing detailed morphological analysis using CellProfiler software. The pictures illustrate the identification of microglia cells using DAPI and Ionized calcium-binding adaptor molecule 1 (IBA1) staining and shows the skeletonization and endpoint definition. **(B)** Representative confocal images of microglia cells ramification in the 3 days group. These images clearly showed a reduction in cell ramification and a transition to amoeboid morphology following the Aβ injection. **(C)** Number of IBA1$^+$ cells at different time points. A significant increase can be seen 12 days after the injection in the Aβ+vehicle treated group. **(D)** Perimeter at different times. The perimeter significantly decreased 3 days after Aβ injection compared to the control group. Perimeter shows a sign of improvement over time. **(E)** Number of branches at different time points. The branch number significantly decreased 3 and 12 days after Aβ injection compared to the control group. **(F)** Number of endpoints at different times. This parameter significantly decreased 3 days after injection compared to the control group. Dehydroepiandrosterone sulfate (DHEAS) and Aβ groups showed similar amoeboid-like morphology, but Iba$^+$ cell numbers resembled controls. Data are expressed as mean± SEM *p<0.05; **p<0.01; ***p<0.001; ****p<0,0001. Sample size is 6–8 animal/group. Scale bar: 10μm.

4 Discussion

Our findings indicated that the Aβ_{1-42} peptide has time-dependent neurotoxic effects on the cholinergic system and the triggered inflammatory response can be one of the contributing factors. Damage to cholinergic neurons became particularly pronounced on day 12, whereas inflammatory responses followed distinct patterns in microglial and astrocyte cells. Microglia activation peaked on day 3 and was gradually reduced afterwards, whereas astrocyte activation was delayed, reaching a peak on day 12. Based on correlations, microglia appear to act as an aggravating factor during the early stage, whereas astrocytes seem to be protective. At later stages, however, astroglia appear to become the detrimental factor. In addition, we confirmed protective DHEAS effects on cholinergic fibers, however its anti-inflammatory properties limited to the area occupied (Figure 3D) and number (Figure 4C) of microglial cells. Thus, anti-inflammatory effects of DHEAS are likely minor, need a prolonged time (not observable at day 3), (Figure 3D) and do not influence glial reactivity caused by mechanical injury (Figure 3B).

Aβ_{1-42} injection into the NBM is a widely used method for modeling neurotoxicity in AD (47). We confirmed the induced cholinergic cell loss and reduced the fiber density in the ipsilateral projection area (SSC), which effect peaked on day 12 post-injection (11). The loss of group differences observed at day 33 may reflect the activation of compensatory mechanisms, e.g. increased AChE activity (48). Several studies have reported up to a 55% reduction in cortical cholinergic fiber density in AD patients (49). Other reports described a marked decrease in cholinergic arborization, particularly in the cortex and hippocampus, which was closely associated with inflammation (50). Thus, the effects of DHEAS on cholinergic fiber density may be critical to AD pathomechanisms, particularly in relation to its anti-inflammatory properties. Our experiment was based on a previous study using a similar protocol with 17β-estradiol (E2) administration, which also led to similar results (i.e., no effect on cholinergic cells and an increase in fiber density in the SSC (11)). We may hypothesize that DHEAS and E2 may act through similar pathways, as DHEAS is a precursor of both estrogen and androgen. However, DHEAS also has a direct, but non-specific affinity for steroid receptors (51–53). In addition,

10.3389/fendo.2026.1764298

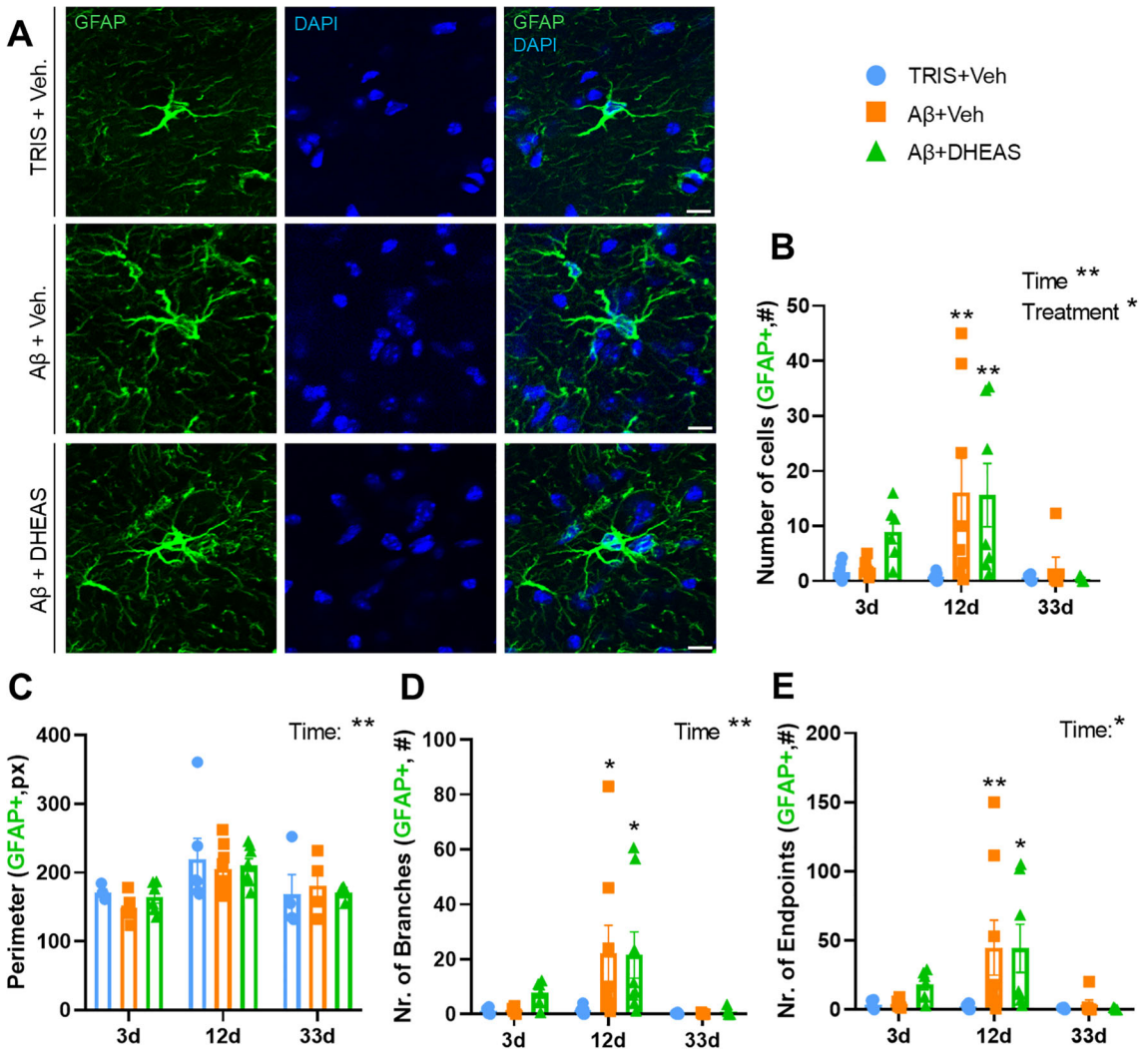


FIGURE 5
Astrocyte (GFAP) cell morphology in the nucleus basalis magnocellularis (NBM): **(A)** Representative confocal images of astrocyte cell anatomy. Increased ramification was detected after both Aβ + Vehicle and Aβ + Dehydroepiandrosterone sulfate (DHEAS) treated groups compared to control. **(B)** Number of glial fibrillary acidic protein (GFAP) positive cells at different time points. Amyloid injection significantly increased the number of cells on a day 12, which was reduced on day 33. **(C)** Perimeter at different times. This parameter showed only time-dependent changes, with the highest values on day 12. **(D)** Number of branches at different time points. The branch number significantly increased 12 days after injection compared to the control group. **(E)** Number of endpoints at the different time points. Number of endpoints significantly increased 12 days after injection. No DHEAS effect was detected, since this group showed the same morphology as the Aβ + Vehicle treated animals. Data are expressed as mean± SEM *p<0.05; **p<0.01. Sample size is 6–8 animal/group. Scale bar: 10μm.

DHEAS likely exerts its effects through non-genomic targets (54). Furthermore, it exhibits direct neuromodulatory effects on both inhibitory (GABAergic) and excitatory (glutamatergic) neurotransmission. Specifically, DHEAS is an allosteric antagonist of $GABA_AR$ receptors (32, 55) and acts as a positive modulator of NMDA receptors (33, 56–58), with specific binding sites (59). The protective effect of DHEAS on fiber density might also be due to its ability to promote the production of NGF and BDNF (34, 60), both directly and via estrogen receptor-mediated pathways (61). Axons and dendrites possess local translation machinery responsive to neurotrophic factors, and BDNF is well known to promote dendritic spine formation, synaptic maintenance, and axonal integrity. Furthermore, DHEAS was recently discovered to maintain synaptic homeostasis and increase spine density (62). In addition, DHEAS can bind to plasma membrane receptors, such as tropomyosin kinase receptor (Trk)-A and p75 neurotrophin receptor (p75NTR), with important roles in proliferation and neuroprotection (31). Moreover, DHEAS may influence microtubule-associated proteins (MAPs), stabilizing microtubules in axons, as evidenced by its binding to the dendritic MAP2C (63). Taken together, these molecular mechanisms may underlie the protective effects of DHEAS on arborization in the cholinergic system. The findings suggest that DHEAS acts locally in axons and dendrites, promoting cytoskeletal stability, enhancing local trophic signaling, scavenging reactive oxygen species, and reducing excitotoxicity. However, it may fail to rescue the soma if nuclear stress pathways, mitochondrial damage, or severe pathology are already present.

The impact of inflammation on the central nervous system depends on its intensity and duration. While brief, controlled

responses are protective, chronic or excessive inflammation may become harmful (64–66). Prolonged exposure to pro-inflammatory molecules further aggravates neurodegeneration (66–68). However, our results indicate a short and controlled inflammatory response, as by day 33 most analyzed parameters had returned to baseline or were similar to control group. This data suggests a potential limitation of this model. Specifically, while chronic, uncontrolled inflammation is a hallmark of AD, the neurotoxic injection in our study induced only a transient inflammatory response. Nevertheless, our findings highlighted the crucial role of glial cells in regulation of the inflammatory response.

The microinjection procedure itself caused mechanical injury, triggering microglial and astrocyte reactivity along the needle tract in the cortex. As no substance was deposited in this region, the observed effects resulted solely from physical trauma. It is well known that traumatic brain injury induces neuronal death and axonal degeneration (69). This is consistent with our findings obtained on day 33 in control animals (injected with TRIS), demonstrating reduced number of $ChAT^+$ cells compared to the control, non-injected site (Figure 2B). The two types of glial cells were activated by the trauma at different times, in line with their distinct functions. Previous studies have shown that microglia activation may precede and influence astrocyte reactivity (70), potentially through the release of cytokines, which in turn enhances astrocytic response (24). Indeed, a recent study has demonstrated that in absence of any external stimuli, microglial activation induces a widespread astrocyte reactivity which is removed after depleting microglia by PLX3997 (71). After the injury, microglia cells immediately migrate to the site of damage to eliminate toxic substances, and this early inflammatory response subsides over time. This data is in line with our results on microglia, which showed increased occupied area and amoeboid morphology already on day 3. In contrast, astrocyte activation begins later and leads to glial scar formation, due to an attempt to restore tissue integrity (72), which we observed on day 12.

In the NBM microglia cells also exhibited earlier reactivity compared to astrocytes (Figures 3D, E). The characterization of microglial morphology in various diseases remains an active area of research (15, 73, 74). Microglia plasticity was already observed by Rıo-Hortega in 1919 (summarized by: (75)) suggesting its two main states: a „resting" state, characterized by highly ramified morphology with limited phagocytic and migratory activity; and an „active" state. The activated microglia adopt an amoeboid shape with increased motility, phagocytic capacity, and proliferative abilities (15, 73, 74). Nonetheless, this duality is being reconsidered in the field, in an attempt of defining the real status of microglia (76). Thus, we analyzed multiple parameters rather than relying on a dual scoring system. Three days after $A\beta_{1-42}$ injection, microglia displayed an amoeboid morphology supported by the increased area occupied, reduced perimeter and number and endpoints of branches (Figure 4). Based upon the positive microglia-cholinergic cell loss correlation at D3 this activated microglia might have contributed to the cholinergic cell loss at D12, which might reflect that transient inflammatory signaling - likely initiated by cytokine and chemokine production - precedes structural damage. Indeed, microglia depletion prevented trauma-induced cognitive decline (77), supporting the damaging role of the microglia at early stages. Interestingly, by day 12, the number of microglia cells increased in the $A\beta_{1-42}$ injected NBM (72), which may suggest a prolonged or secondary inflammatory response to the toxic substance. This may be explained by the fact that Aβ toxicity was insufficient to induce microglial death, allowing surviving cells to remain active and proliferate through IL-1β–mediated trophic signaling (78).

Similar to microglia, the reactivity states and molecular profiles of astrocyte cells also exhibit a transition, depending on the extent of damage and inflammation (17, 79, 80). During reactivity, they show hypertrophy, with an increase in both their size and the number of branching in their processes (17–19). In the resting state, an astrocyte has fewer processes and shows low GFAP expression (79, 81). Additionally, non-reactive astrocytes are spaced farther apart with minimal overlap (17). In the case of severe injury, neurodegenerative effects, or chronic inflammation, reactive astrogliosis is characterized by a significant increase in gene expression and cellular hypertrophy (17, 80). The data obtained in our study is consistent with the literature as $A\beta_{1-42}$ injection increased the number of astrocytes, branches, and endpoints (Figure 5), indicating a more ramified morphology 12 days post-injection. Although the observed morphological alterations suggest increased glial reactivity, future studies incorporating mRNA and protein markers (e.g., *Il1b*, *Tnfa*, *Trem2*, *Clec7a*, *Cd45*) are warranted to provide a more comprehensive characterization of glial activation beyond morphology. Interestingly, the early negative and later positive correlations between astrocyte markers and cholinergic cell loss suggest a shift in astrocyte function from an initially protective role to a later detrimental one. Several studies support the protective role of astrocytes (82), which may subsequently transition to a harmful phenotype (83), presumably due to activation by microglia (84, 85). Thus, the observed changes might represent apadtive, rather than compensatory responses.

DHEAS treated group often displayed outcomes indistinguishable from the Aβ+Veh. group, whereas mild anti-inflammatory effects of DHEAS were primarily observed on day 12. Previous findings suggested that DHEAS anti-inflammatory effects (24) could be exerted via binding to TrkA receptors and activation of protein kinase B/cAMP response element-binding protein (AKT/CREB) pathway. This indirectly inhibits the expression of inflammatory genes and reduces secretion of pro-inflammatory cytokines from microglia (30). Furthermore, DHEA has been shown to induce JMJD3 (an inflammation-sensitive histone demethylase) expression and promote an anti-inflammatory microglial phenotype in hemoglobin-induced neuroinflammation (86). Through its action on oligodendroglia cells, DHEAS may reduce demyelination and axon loss. Moreover, DHEAS was also shown to decrease IL-1β and interferon-gamma (IFNγ) levels in the spinal cord (87). After being transformed into androstenediol, DHEAS can modulate estrogen receptor β, thereby suppressing the inflammatory response of glia cells (88). It has been reported to exert antioxidant effects in microglia, as it reduces LPS-induced nitrite production and iNOS protein expression, suggesting a post-transcriptional mechanism that limits reactive nitrogen species generation (89). Chronic DHEA treatment - similar to a

single DHEA dose - reduced cocaine-induced astroglia volume in the dentate gyrus of rats (90). Another possible molecular effect of DHEA is the enhancement of glutamate uptake by astrocytes, by promoting the insertion of the glutamate transporter (GLT-1) into the cell membrane (91). Previous studies have shown that DHEAS can reduce reactive astrocytes, as indicated by decreased S100β-positive cells in a cocaine self-administration model (90) and attenuate astroglial activation in an iron-induced post-traumatic epilepsy model (92). In our study, the lack of detectable GFAP morphological changes may reflect the treatment window used. Moreover, functional or biochemical changes, such as cytokine secretion, may occur without detectable morphological alterations (79, 93). Future studies using chronic or later administration, as well as complementary functional or molecular markers (e.g., S100β or ALDH1L1), could provide additional insight into astrocytic modulation by DHEAS. Furthermore, DHEAS may shift the excitatory/inhibitory balance, indirectly influencing microglial activation and astrocytic metabolic and inflammatory responses, as both glial cell types are highly sensitive to neuronal activity patterns (94, 95). This mechanism may counteract the anti-inflammatory effect of DHEA masking any changes. DHEA also appears to reduce astroglia activation following denervation, although this may partly be due to its conversion into estrogen (96). All in all, previous findings suggest that glial cells may play a central role in mediating the effects of DHEAS. The limited effectiveness of DHEAS administration in our study might be due to the timing or characteristics of the treatment.

Since, besides Aβ, tau hyperphosphorylation also plays a central role in the pathomechanism of AD, it is important to assess our results in the context of tau pathology. Tau accumulation in basal forebrain cholinergic neurons inhibits their firing, and number, and extracellular tau may increase this loss via interactions with M1/M3 muscarinic receptors (97–99). Furthermore, transgenic mouse models expressing various pathological pTau mutations exhibited a reduction in ChAT-positive basal forebrain neurons, concomitant with impairments in spatial learning and enhanced microglial activation (50). Notably, microglia-driven inflammation not only responds to tau pathology but also actively promotes it, driving the progression of tauopathies and facilitating the spreading of pathological tau throughout the brain (100, 101). Additionally, tau might induce proinflammatory astrocytic activation (102), which might also contribute to neurodegeneration (103). In relation to DHEA, its *in vitro* administration elevated the level of Tau, but not its phosphorylation (104), questioning their interaction.

In summary, $A\beta_{1-42}$ administration demonstrated a neurotoxic effect, as evidenced by the reduced number of $ChAT^+$ cells in the NBM and their decreased projections in the SSC. The time-dependent microglial cell activation in the NBM may precede, and aggravate the process. DHEAS protective actions against Aβ-neurotoxicity were observed on day 12 on the cholinergic fibers, with mild anti-inflammatory effects on glial cells. Our findings primarily contribute to the better understanding of complex AD pathogenesis in a histological level, while also suggesting therapeutic potential of DHEAS. However, additional studies are required to substantiate this possibility.

Data availability statement

The raw data supporting the conclusions of this article will be made available by the authors, without undue reservation.

Ethics statement

The animal study was approved by Workplace Animal Welfare Committee of the University of Pécs and the National Scientific Ethical Committee on Animal Experimentation of Hungary (BA02/2000-84/2022). The study was conducted in accordance with the local legislation, institutional requirements and performed according to the European Community Council Directive recommendations for the care and use of laboratory animals (2010/63/EU).

Author contributions

CS: Conceptualization, Data curation, Investigation, Methodology, Visualization, Formal Analysis, Writing – original draft. GM: Methodology, Software, Formal Analysis, Writing – review & editing. NC-C: Methodology, Investigation, Formal Analysis, Writing – review & editing. DS: Writing – review & editing, Funding acquisition, Supervision. DZ: Writing – review & editing, Conceptualization, Investigation, Methodology, Supervision, Funding acquisition, Resources. SF: Project administration, Formal Analysis, Writing – original draft, Visualization, Data curation, Methodology, Investigation, Resources, Conceptualization.

Funding

The author(s) declared that financial support was received for this work and/or its publication. This research was conducted with the support of the National Academy of Scientist Education Program of the National Biomedical Foundation under the sponsorship of the Hungarian Ministry of Culture and Innovation (FEIF/646-4/2021- ITM_SZERZ). Furthermore, this work was also supported by New National Excellence Program (ÚNKP-23-2-II-PTE-1858) and University Research Fellowship (EKÖP-24-2-I-PTE-63) of the Hungarian Ministry for Culture and Innovation, National Research Development and Innovation Office, as well as by the Croatian Ministry of Science and Education, Croatian-Hungarian bilateral project "Testing dehydroepiandrosterone as possible treatment for Alzheimer's disorder using *in vitro* and *in vivo* models". Additional support came from the National Brain Research Program (NAP 3.0) of the Hungarian Academy of Sciences; the National Research Development and Innovation Office of Hungary (grant numbers K141934 and K138763); and the Thematic Excellence Program 2021 Health Subprogram of the Ministry for Innovation and Technology in Hungary within the framework of the TKP2021-EGA-16 project of Pécs University.

Acknowledgments

The research was performed in collaboration with the Ábrahám István Nano-Bio-Imaging Core Facility at the University of Pécs.

Conflict of interest

The author(s) declared that this work was conducted in the absence of any commercial or financial relationships that could be construed as a potential conflict of interest.

Generative AI statement

The author(s) declared that generative AI was not used in the creation of this manuscript.

Any alternative text (alt text) provided alongside figures in this article has been generated by Frontiers with the support of artificial intelligence and reasonable efforts have been made to ensure accuracy, including review by the authors wherever possible. If you identify any issues, please contact us.

Publisher's note

All claims expressed in this article are solely those of the authors and do not necessarily represent those of their affiliated organizations, or those of the publisher, the editors and the reviewers. Any product that may be evaluated in this article, or claim that may be made by its manufacturer, is not guaranteed or endorsed by the publisher.

Supplementary material

The Supplementary Material for this article can be found online at: https://www.frontiersin.org/articles/10.3389/fendo.2026.1764298/full#supplementary-material

References

1. Lewis PR, Shute CC. The cholinergic limbic system: projections to hippocampal formation, medial cortex, nuclei of the ascending cholinergic reticular system, and the subfornical organ and supra-optic crest. *Brain*. (1967) 90:521–40. doi: 10.1093/brain/90.3.521

2. Ferreira-Vieira TH, Guimaraes IM, Silva FR, Ribeiro FM. Alzheimer's disease: targeting the cholinergic system. *Curr Neuropharmacol*. (2016) 14:101–15. doi: 10.2174/1570159x13666150716165726

3. Whitehouse PJ, Price DL, Struble RG, Clark AW, Coyle JT, Delon MR. Alzheimer's disease and senile dementia: loss of neurons in the basal forebrain. *Science*. (1982) 215:1237–9. doi: 10.1126/science.7058341

4. Hanna Al-Shaikh FS, Duara R, Crook JE, Lesser ER, Schaeverbeke J, Hinkle KM, et al. Selective vulnerability of the nucleus basalis of meynert among neuropathologic subtypes of alzheimer disease. *JAMA Neurol*. (2020) 77:225–33. doi: 10.1001/jamaneurol.2019.3606

5. Thal DR, Rub U, Orantes M, Braak H. Phases of A beta-deposition in the human brain and its relevance for the development of AD. *Neurology*. (2002) 58:1791–800. doi: 10.1212/WNL.58.12.1791

6. Xie K, Ryan D, Schroder S, Freund L, Bonn S, Zhou Y, et al. Selective vulnerability of the aging cholinergic system to amyloid pathology revealed by induced APP overexpression. *J Neuroinflamm*. (2026) 23:39. doi: 10.1186/s12974-025-03682-2

7. Lehericy S, Hirsch EC, Cervera-Pierot P, Hersh LB, Bakchine S, Piette F, et al. Heterogeneity and selectivity of the degeneration of cholinergic neurons in the basal forebrain of patients with Alzheimer's disease. *J Comp Neurol*. (1993) 330:15–31. doi: 10.1002/cne.903300103

8. Blusztajn JK, Berse B. The cholinergic neuronal phenotype in Alzheimer's disease. *Metab Brain Dis*. (2000) 15:45–64. doi: 10.1007/BF02680013

9. De Ferrari GV, Canales MA, Shin I, Weiner LM, Silman I, Inestrosa NC. A structural motif of acetylcholinesterase that promotes amyloid beta-peptide fibril formation. *Biochemistry*. (2001) 40:10447–57. doi: 10.1021/bi0101392

10. Harkany T, Abraham I, Konya C, Nyakas C, Zarandi M, Penke B, et al. Mechanisms of beta-amyloid neurotoxicity: perspectives of pharmacotherapy. *Rev Neurosci*. (2000) 11:329–82. doi: 10.1515/REVNEURO.2000.11.4.329

11. Kwakowsky A, Potapov K, Kim S, Peppercorn K, Tate WP, Abraham IM. Treatment of beta amyloid 1-42 (Abeta(1-42))-induced basal forebrain cholinergic damage by a non-classical estrogen signaling activator *in vivo*. *Sci Rep*. (2016) 6:21101. doi: 10.1038/srep21101

12. Uddin MS, Lim LW. Glial cells in Alzheimer's disease: From neuropathological changes to therapeutic implications. *Ageing Res Rev*. (2022) 78:101622. doi: 10.1016/j.arr.2022.101622

13. Singh D. Astrocytic and microglial cells as the modulators of neuroinflammation in Alzheimer's disease. *J Neuroinflamm*. (2022) 19:206. doi: 10.1186/s12974-022-02565-0

14. Hammond TR, Dufort C, Dissing-Olesen L, Giera S, Young A, Wysoker A, et al. Single-cell RNA sequencing of microglia throughout the mouse lifespan and in the injured brain reveals complex cell-state changes. *Immunity*. (2019) 50:253–271.e6. doi: 10.1016/j.immuni.2018.11.004

15. Vidal-Itriago A, Radford RAW, Aramideh JA, Maurel C, Scherer NM, Don EK, et al. Microglia morphophysiological diversity and its implications for the CNS. *Front Immunol*. (2022) 13:997786. doi: 10.3389/fimmu.2022.997786

16. Al-Ghraiybah NF, Wang J, Alkhalifa AE, Roberts AB, Raj R, Yang E, et al. Glial cell-mediated neuroinflammation in alzheimer's disease. *Int J Mol Sci*. (2022) 23:10572. doi: 10.3390/ijms231810572

17. Dossi E, Vasile F, Rouach N. Human astrocytes in the diseased brain. *Brain Res Bull*. (2018) 136:139–56. doi: 10.1016/j.brainresbull.2017.02.001

18. Baldwin KT, Murai KK, Khakh BS. Astrocyte morphology. *Trends Cell Biol*. (2024) 34:547–65. doi: 10.1016/j.tcb.2023.09.006

19. Pekny M, Wilhelmsson U, Pekna M. The dual role of astrocyte activation and reactive gliosis. *Neurosci Lett*. (2014) 565:30–8. doi: 10.1016/j.neulet.2013.12.071

20. Verkhratsky A, Butt A, Li B, Illes P, Zorec R, Semyanov A, et al. Astrocytes in human central nervous system diseases: a frontier for new therapies. *Signal Transduct Target Ther*. (2023) 8:396. doi: 10.1038/s41392-023-01628-9

21. Maninger N, Wolkowitz OM, Reus VI, Epel ES, Mellon SH. Neurobiological and neuropsychiatric effects of dehydroepiandrosterone (DHEA) and DHEA sulfate (DHEAS). *Front Neuroendocrinol*. (2009) 30:65–91. doi: 10.1016/j.yfrne.2008.11.002

22. Auchus RJ. Overview of dehydroepiandrosterone biosynthesis. *Semin Reprod Med*. (2004) 22:281–8. doi: 10.1055/s-2004-861545

23. Zwain IH, Yen SS. Neurosteroidogenesis in astrocytes, oligodendrocytes, and neurons of cerebral cortex of rat brain. *Endocrinology*. (1999) 140:3843–52. doi: 10.1210/endo.140.8.6907

24. Yilmaz C, Karali K, Fodelianaki G, Gravanis A, Chavakis T, Charalampopoulos I, et al. Neurosteroids as regulators of neuroinflammation. *Front Neuroendocrinol*. (2019) 55:100788. doi: 10.1016/j.yfrne.2019.100788

25. Tannenbaum C, Barrett-Connor E, Laughlin GA, Platt RW. A longitudinal study of dehydroepiandrosterone sulphate (DHEAS) change in older men and women: the Rancho Bernardo Study. *Eur J Endocrinol*. (2004) 151:717–25. doi: 10.1530/eje.0.1510717

26. Pan X, Wu X, Kaminga AC, Wen SW, Liu A. Dehydroepiandrosterone and dehydroepiandrosterone sulfate in alzheimer's disease: A systematic review and meta-analysis. *Front Aging Neurosci*. (2019) 11:61. doi: 10.3389/fnagi.2019.00061

27. Aldred S, Mecocci P. Decreased dehydroepiandrosterone (DHEA) and dehydroepiandrosterone sulfate (DHEAS) concentrations in plasma of Alzheimer's disease (AD) patients. *Arch Gerontol Geriatr*. (2010) 51:e16–8. doi: 10.1016/j.archger.2009.07.001

28. Hillen T, Lun A, Reischies FM, Borchelt M, Steinhagen-Thiessen E, Schaub RT. DHEA-S plasma levels and incidence of Alzheimer's disease. *Biol Psychiatry*. (2000) 47:161–3. doi: 10.1016/S0006-3223(99)00217-6

29. Vuic B, Milos T, Kvak E, Konjevod M, Tudor L, Farkas S, et al. Neuroprotective effects of dehydroepiandrosterone sulphate against abeta toxicity and accumulation in cellular and animal model of alzheimer's disease. *Biomedicines*. (2025) 13:432. doi: 10.3390/biomedicines13020432

30. Alexaki VI, Fodelianaki G, Neuwirth A, Mund C, Kourgiantaki A, Ieronimaki E, et al. DHEA inhibits acute microglia-mediated inflammation through activation of the TrkA-Akt1/2-CREB-Jmjd3 pathway. *Mol Psychiatry*. (2018) 23:1410–20. doi: 10.1038/mp.2017.167

31. Lazaridis I, Charalampopoulos I, Alexaki VI, Avlonitis N, Pediaditakis I, Efstathopoulos P, et al. Neurosteroid dehydroepiandrosterone interacts with nerve growth factor (NGF) receptors, preventing neuronal apoptosis. *PloS Biol*. (2011) 9: e1001051. doi: 10.1371/journal.pbio.1001051

32. Svob Strac D, Jazvinscak Jembrek M, Erhardt J, Mirkovic Kos K, Pericic D. Modulation of recombinant GABA(A) receptors by neurosteroid dehydroepiandrosterone sulfate. *Pharmacology*. (2012) 89:163–71. doi: 10.1159/000336058

33. Johansson T, Elfverson M, Zhou Q, Nyberg F. Allosteric modulation of the NMDA receptor by neurosteroids in rat brain and the impact of long term morphine administration. *Biochem Biophys Res Commun*. (2010) 401:504–8. doi: 10.1016/j.bbrc.2010.09.073

34. Rahmani A, Shoae-Hassani A, Keyhanvar P, Kheradmand D, Darbandi-Azar A. Dehydroepiandrosterone stimulates nerve growth factor and brain derived neurotrophic factor in cortical neurons. *Adv Pharmacol Sci*. (2013) 2013:506191. doi: 10.1155/2013/506191

35. Rhodes ME, Li PK, Flood JF, Johnson DA. Enhancement of hippocampal acetylcholine release by the neurosteroid dehydroepiandrosterone sulfate: an *in vivo* microdialysis study. *Brain Res*. (1996) 733:284–6. doi: 10.1016/0006-8993(96)00751-2

36. Rhodes ME, Li PK, Burke AM, Johnson DA. Enhanced plasma DHEAS, brain acetylcholine and memory mediated by steroid sulfatase inhibition. *Brain Res*. (1997) 773:28–32. doi: 10.1016/S0006-8993(97)00867-6

37. Maggio M, De Vita F, Fisichella A, Colizzi E, Provenzano S, Lauretani F, et al. DHEA and cognitive function in the elderly. *J Steroid Biochem Mol Biol*. (2015) 145:281–92. doi: 10.1016/j.jsbmb.2014.03.014

38. Floden AM, Li S, Combs CK. Beta-amyloid-stimulated microglia induce neuron death via synergistic stimulation of tumor necrosis factor alpha and NMDA receptors. *J Neurosci*. (2005) 25:2566–75. doi: 10.1523/JNEUROSCI.4998-04.2005

39. Friedrich N, Volzke H, Rosskopf D, Steveling A, Krebs A, Nauck M, et al. Reference ranges for serum dehydroepiandrosterone sulfate and testosterone in adult men. *J Androl*. (2008) 29:610–7. doi: 10.2164/jandrol.108.005561

40. Lehmann J, Nagy JI, Atmadia S, Fibiger HC. The nucleus basalis magnocellularis: the origin of a cholinergic projection to the neocortex of the rat. *Neuroscience*. (1980) 5:1161–74. doi: 10.1016/0306-4522(80)90195-5

41. Tsui KC, Roy J, Chau SC, Wong KH, Shi L, Poon CH, et al. Distribution and inter-regional relationship of amyloid-beta plaque deposition in a 5xFAD mouse model of Alzheimer's disease. *Front Aging Neurosci*. (2022) 14:964336. doi: 10.3389/fnagi.2022.964336

42. Javonillo DI, Tran KM, Phan J, Hingco E, Kramar EA, da Cunha C, et al. Systematic phenotyping and characterization of the 3xTg-AD mouse model of alzheimer's disease. *Front Neurosci*. (2021) 15:785276. doi: 10.3389/fnins.2021.785276

43. Perez SE, He B, Muhammad N, Oh KJ, Fahnestock M, Ikonomovic MD, et al. Cholinotrophic basal forebrain system alterations in 3xTg-AD transgenic mice. *Neurobiol Dis*. (2011) 41:338–52. doi: 10.1016/j.nbd.2010.10.002

44. Arendt T, Taubert G, Bigl V, Arendt A. Amyloid deposition in the nucleus basalis of Meynert complex: a topographic marker for degenerating cell clusters in Alzheimer's disease. *Acta Neuropathol*. (1988) 75:226–32. doi: 10.1007/BF00690530

45. George Paxinos KBJF. *The Mouse Brain in Stereotaxic Coordinates*. San Diego (CA): Academic Press. (2001).

46. Koszegi Z, Szego EM, Cheong RY, Tolod-Kemp E, Abraham IM. Postlesion estradiol treatment increases cortical cholinergic innervations via estrogen receptor-alpha dependent nonclassical estrogen signaling *in vivo*. *Endocrinology*. (2011) 152:3471–82. doi: 10.1210/en.2011-1017

47. Calvo-Flores Guzman B, Elizabeth Chaffey T, Hansika Palpagama T, Waters S, Boix J, Tate WP, et al. The interplay between beta-amyloid 1-42 (Abeta(1-42))-induced hippocampal inflammatory response, p-tau, vascular pathology, and their synergistic contributions to neuronal death and behavioral deficits. *Front Mol Neurosci*. (2020) 13:522073. doi: 10.3389/fnmol.2020.552073

48. Bronfman FC, Moechars D, Van Leuven F. Acetylcholinesterase-positive fiber deafferentation and cell shrinkage in the septohippocampal pathway of aged amyloid precursor protein london mutant transgenic mice. *Neurobiol Dis*. (2000) 7:152–68. doi: 10.1006/nbdi.2000.0283

49. Geula C, Mesulam MM. Systematic regional variations in the loss of cortical cholinergic fibers in Alzheimer's disease. *Cereb Cortex*. (1996) 6:165–77. doi: 10.1093/cercor/6.2.165

50. Cranston AL, Wysocka A, Steczkowska M, Zadrozny M, Palasz E, Harrington CR, et al. Cholinergic and inflammatory phenotypes in transgenic tau mouse models of Alzheimer's disease and frontotemporal lobar degeneration. *Brain Commun*. (2020) 2: fcaa033. doi: 10.1093/braincomms/fcaa033

51. Chen F, Knecht K, Birzin E, Fisher J, Wilkinson H, Mojena M, et al. Direct agonist/antagonist functions of dehydroepiandrosterone. *Endocrinology*. (2005) 146:4568–76. doi: 10.1210/en.2005-0368

52. Teng Y, Litchfield LM, Ivanova MM, Prough RA, Clark BJ, Klinge CM. Dehydroepiandrosterone-induces miR-21 transcription in HepG2 cells through estrogen receptor beta and androgen receptor. *Mol Cell Endocrinol*. (2014) 392:23–36. doi: 10.1016/j.mce.2014.05.007

53. Webb SJ, Geoghegan TE, Prough RA, Michael Miller KK. The biological actions of dehydroepiandrosterone involves multiple receptors. *Drug Metab Rev*. (2006) 38:89–116. doi: 10.1080/03602530600569877

54. Weng JH, Chung BC. Nongenomic actions of neurosteroid pregnenolone and its metabolites. *Steroids*. (2016) 111:54–9. doi: 10.1016/j.steroids.2016.01.017

55. Demirgoren S, Majewska MD, Spivak CE, London ED. Receptor binding and electrophysiological effects of dehydroepiandrosterone sulfate, an antagonist of the GABAA receptor. *Neuroscience*. (1991) 45:127–35. doi: 10.1016/0306-4522(91)90109-2

56. Bergeron R, de Montigny C, Debonnel G. Potentiation of neuronal NMDA response induced by dehydroepiandrosterone and its suppression by progesterone: effects mediated via sigma receptors. *J Neurosci*. (1996) 16:1193–202. doi: 10.1523/JNEUROSCI.16-03-01193.1996

57. Zoupa E, Gravanis A, Pitsikas N. The novel dehydroepiandrosterone (DHEA) derivative BNN27 counteracts behavioural deficits induced by the NMDA receptor antagonist ketamine in rats. *Neuropharmacology*. (2019) 151:74–83. doi: 10.1016/j.neuropharm.2019.04.001

58. Pitsikas N, Zoupa E, Gravanis A. The novel dehydroepiandrosterone derivative BNN27 counteracts the impairing effects of anesthetic ketamine on rats' non-spatial and spatial recognition memory. *Behav Brain Res*. (2022) 430:113937. doi: 10.1016/j.bbr.2022.113937

59. Qian M, Xu Y, Shu HJ, Chen ZW, Wang L, Zorumski CF, et al. Synthesis and evaluation of photoaffinity labeling reagents for identifying binding sites of sulfated neurosteroids on NMDA and GABA(A) receptors. *RSC Adv*. (2024) 14:36352–69. doi: 10.1039/D4RA07074G

60. Naylor JC, Hulette CM, Steffens DC, Shampine LJ, Ervin JF, Payne VM, et al. Cerebrospinal fluid dehydroepiandrosterone levels are correlated with brain dehydroepiandrosterone levels, elevated in Alzheimer's disease, and related to neuropathological disease stage. *J Clin Endocrinol Metab*. (2008) 93:3173–8. doi: 10.1210/jc.2007-1229

61. Murphy DD, Cole NB, Segal M. Brain-derived neurotrophic factor mediates estradiol-induced dendritic spine formation in hippocampal neurons. *Proc Natl Acad Sci U.S.A*. (1998) 95:11412–7. doi: 10.1073/pnas.95.19.11412

62. Luine V, Mohan G, Attalla S, Jacome L, Frankfurt M. Androgens enhance recognition memory and dendritic spine density in the hippocampus and prefrontal cortex of ovariectomized female rats. *Neuroscience*. (2025) 568:465–75. doi: 10.1016/j.neuroscience.2022.06.002

63. Laurine E, Lafitte D, Gregoire C, Seree E, Loret E, Douillard S, et al. Specific binding of dehydroepiandrosterone to the N terminus of the microtubule-associated protein MAP2. *J Biol Chem*. (2003) 278:29979–86. doi: 10.1074/jbc.M303242200

64. DiSabato DJ, Quan N, Godbout JP. Neuroinflammation: the devil is in the details. *J Neurochem*. (2016) 139 Suppl 2:136–53. doi: 10.1111/jnc.13607

65. Kwon HS, Koh SH. Neuroinflammation in neurodegenerative disorders: the roles of microglia and astrocytes. *Transl Neurodegener*. (2020) 9:42. doi: 10.1186/s40035-020-00221-2

66. Wyss-Coray T, Mucke L. Inflammation in neurodegenerative disease–a double-edged sword. *Neuron*. (2002) 35:419–32. doi: 10.1016/S0896-6273(02)00794-8

67. Heneka MT, Carson MJ, El Khoury J, Landreth GE, Brosseron F, Feinstein DL, et al. Neuroinflammation in alzheimer's disease. *Lancet Neurol*. (2015) 14:388–405. doi: 10.1016/S1474-4422(15)70016-5

68. Norden DM, Godbout JP. Review: microglia of the aged brain: primed to be activated and resistant to regulation. *Neuropathol Appl Neurobiol*. (2013) 39:19–34. doi: 10.1111/j.1365-2990.2012.01306.x

69. Greenhalgh AD, David S, Bennett FC. Immune cell regulation of glia during CNS injury and disease. *Nat Rev Neurosci*. (2020) 21:139–52. doi: 10.1038/s41583-020-0263-9

70. Belfiore R, Rodin A, Ferreira E, Velazquez R, Branca C, Caccamo A, et al. Temporal and regional progression of Alzheimer's disease-like pathology in 3xTg-AD mice. *Aging Cell*. (2019) 18:e12873. doi: 10.1111/acel.12873

71. Mora-Romero B, Capelo-Carrasco N, Perez-Moreno JJ, Alvarez-Vergara MI, Trujillo-Estrada L, Romero-Molina C, et al. Microglia mitochondrial complex I deficiency during development induces glial dysfunction and early lethality. *Nat Metab*. (2024) 6:1479–91. doi: 10.1038/s42255-024-01081-0

72. Arbo BD, Bennetti F, Ribeiro MF. Astrocytes as a target for neuroprotection: Modulation by progesterone and dehydroepiandrosterone. *Prog Neurobiol*. (2016) 144:27–47. doi: 10.1016/j.pneurobio.2016.03.010

73. Beynon SB, Walker FR. Microglial activation in the injured and healthy brain: what are we really talking about? Practical and theoretical issues associated with the measurement of changes in microglial morphology. *Neuroscience*. (2012) 225:162–71. doi: 10.1016/j.neuroscience.2012.07.029

74. Walker FR, Beynon SB, Jones KA, Zhao Z, Kongsui R, Cairns M, et al. Dynamic structural remodelling of microglia in health and disease: a review of the models, the signals and the mechanisms. *Brain Behav Immun*. (2014) 37:1–14. doi: 10.1016/j.bbi.2013.12.010

75. Sierra A, de Castro F, Del Rio-Hortega J, Rafael Iglesias-Rozas J, Garrosa M, Kettenmann H. The "Big-Bang" for modern glial biology: Translation and comments on Pio del Rio-Hortega 1919 series of papers on microglia. *Glia*. (2016) 64:1801–40. doi: 10.1002/glia.23046

76. Paolicelli RC, Sierra A, Stevens B, Tremblay ME, Aguzzi A, Ajami B, et al. Microglia states and nomenclature: A field at its crossroads. *Neuron*. (2022) 110:3458–83. doi: 10.1016/j.neuron.2022.10.020

77. Delcy SAS, Farrugia A, Diaz Nieves IA, O'Brien CA, Bennett FC, Cohen AS. Microglia depletion improves hippocampal circuit function after mild traumatic brain injury in male mice. *Brain Behav Immun*. (2026) 131:106178. doi: 10.1016/j.bbi.2025.106178

78. Prinz M, Jung S, Priller J. Microglia biology: one century of evolving concepts. *Cell*. (2019) 179:292–311. doi: 10.1016/j.cell.2019.08.053

79. Sofroniew MV, Vinters HV. Astrocytes: biology and pathology. *Acta Neuropathol*. (2010) 119:7–35. doi: 10.1007/s00401-009-0619-8

80. Sofroniew MV. Molecular dissection of reactive astrogliosis and glial scar formation. *Trends Neurosci*. (2009) 32:638–47. doi: 10.1016/j.tins.2009.08.002

81. Eng LF, Ghirnikar RS, Lee YL. Glial fibrillary acidic protein: GFAP-thirty-one years (1969-2000). *Neurochem Res*. (2000) 25:1439–51. doi: 10.1023/A:1007677003387

82. Sofroniew MV. Reactive astrocytes in neural repair and protection. *Neuroscientist*. (2005) 11:400–7. doi: 10.1177/1073858405278321

83. Ding ZB, Song LJ, Wang Q, Kumar G, Yan YQ, Ma CG. Astrocytes: a double-edged sword in neurodegenerative diseases. *Neural Regener Res*. (2021) 16:1702–10. doi: 10.4103/1673-5374.306064

84. Liddelow SA, Guttenplan KA, Clarke LE, Bennett FC, Bohlen CJ, Schirmer L, et al. Neurotoxic reactive astrocytes are induced by activated microglia. *Nature*. (2017) 541:481–7. doi: 10.1038/nature21029

85. Li T, Liu T, Chen X, Li L, Feng M, Zhang Y, et al. Microglia induce the transformation of A1/A2 reactive astrocytes via the CXCR7/PI3K/Akt pathway in chronic post-surgical pain. *J Neuroinflamm*. (2020) 17:211. doi: 10.1186/s12974-020-01891-5

86. Tao T, Liu GJ, Shi X, Zhou Y, Lu Y, Gao YY, et al. DHEA attenuates microglial activation via induction of JMJD3 in experimental subarachnoid haemorrhage. *J Neuroinflamm*. (2019) 16:243. doi: 10.1186/s12974-019-1641-y

87. Boghozian R, McKenzie BA, Saito LB, Mehta N, Branton WG, Lu J, et al. Suppressed oligodendrocyte steroidogenesis in multiple sclerosis: Implications for regulation of neuroinflammation. *Glia*. (2017) 65:1590–606. doi: 10.1002/glia.23179

88. Aggelakopoulou M, Kourepini E, Paschalidis N, Simoes DC, Kalavrizioti D, Dimisianos N, et al. ERbeta-dependent direct suppression of human and murine th17 cells and treatment of established central nervous system autoimmunity by a neurosteroid. *J Immunol*. (2016) 197:2598–609. doi: 10.4049/jimmunol.1601038

89. Barger SW, Chavis JA, Drew PD. Dehydroepiandrosterone inhibits microglial nitric oxide production in a stimulus-specific manner. *J Neurosci Res*. (2000) 62:503–9. doi: 10.1002/1097-4547(20001115)62:4<503::AID-JNR4>3.0.CO;2-A

90. Ahdoot-Levi H, Croitoru O, Bareli T, Sudai E, Peer-Nissan H, Jacob A, et al. The effect of dehydroepiandrosterone treatment on neurogenesis, astrogliosis and long-term cocaine-seeking behavior in a cocaine self-administration model in rats. *Front Neurosci*. (2021) 15:773197. doi: 10.3389/fnins.2021.773197

91. Chen T, Tanaka M, Wang Y, Sha S, Furuya K, Chen L, et al. Neurosteroid dehydroepiandrosterone enhances activity and trafficking of astrocytic GLT-1 via sigma(1) receptor-mediated PKC activation in the hippocampal dentate gyrus of rats. *Glia*. (2017) 65:1491–503. doi: 10.1002/glia.23175

92. Prakash C, Rabidas SS, Tyagi J, Sharma D. Dehydroepiandrosterone attenuates astroglial activation, neuronal loss and dendritic degeneration in iron-induced post-traumatic epilepsy. *Brain Sci*. (2023) 13:563. doi: 10.3390/brainsci13040563

93. Escartin C, Galea E, Lakatos A, O'Callaghan JP, Petzold GC, Serrano-Pozo A, et al. Reactive astrocyte nomenclature, definitions, and future directions. *Nat Neurosci*. (2021) 24:312–25. doi: 10.1038/s41593-020-00783-4

94. Van Horn MR, Benfey NJ, Shikany C, Severs LJ, Deemyad T. Neuron-astrocyte networking: astrocytes orchestrate and respond to changes in neuronal network activity across brain states and behaviors. *J Neurophysiol*. (2021) 126:627–36. doi: 10.1152/jn.00062.2021

95. Pena-Ortega F. Microglial modulation of neuronal network function and plasticity. *J Neurophysiol*. (2025) 133:661–80. doi: 10.1152/jn.00458.2024

96. Hoyk Z, Parducz A, Garcia-Segura LM. Dehydroepiandrosterone regulates astroglia reaction to denervation of olfactory glomeruli. *Glia*. (2004) 48:207–16. doi: 10.1002/glia.20070

97. Vana L, Kanaan NM, Ugwu IC, Wuu J, Mufson EJ, Binder LI. Progression of tau pathology in cholinergic Basal forebrain neurons in mild cognitive impairment and Alzheimer's disease. *Am J Pathol*. (2011) 179:2533–50. doi: 10.1016/j.ajpath.2011.07.044

98. Wu D, Yu N, Gao Y, Xiong R, Liu L, Lei H, et al. Targeting a vulnerable septum-hippocampus cholinergic circuit in a critical time window ameliorates tau-impaired memory consolidation. *Mol Neurodegener*. (2023) 18:23. doi: 10.1186/s13024-023-00614-7

99. Simon D, Hernandez F, Avila J. The involvement of cholinergic neurons in the. *spreading tau pathology. Front Neurol*. (2013) 4:74. doi: 10.3389/fneur.2013.00074

100. Lee SH, Bae EJ, Park SJ, Lee SJ. Microglia-driven inflammation induces progressive tauopathies and synucleinopathies. *Exp Mol Med*. (2025) 57:1017–31. doi: 10.1038/s12276-025-01450-z

101. Maphis N, Xu G, Kokiko-Cochran ON, Jiang S, Cardona A, Ransohoff RM, et al. Reactive microglia drive tau pathology and contribute to the spreading of pathological tau in the brain. *Brain*. (2015) 138:1738–55. doi: 10.1093/brain/awv081

102. Wang P, Anderson DE, Ye Y. PI3K-AKT activation resculpts integrin signaling to drive filamentous tau-induced proinflammatory astrogliosis. *Res Sq*. (2023) 13:179. doi: 10.2139/ssrn.4488577

103. Wang C, Xiong M, Gratuze M, Bao X, Shi Y, Andhey PS, et al. Selective removal of astrocytic APOE4 strongly protects against tau-mediated neurodegeneration and decreases synaptic phagocytosis by microglia. *Neuron*. (2021) 109:1657–1674.e7. doi: 10.1016/j.neuron.2021.03.024

104. Konsta V, Paschou M, Koti N, Vlachou ME, Livanos P, Xilouri M, et al. Neurosteroids alter p-ERK levels and tau distribution, restraining the effects of high extracellular calcium. *Int J Mol Sci*. (2024) 25:11637. doi: 10.3390/ijms252111637